Available online at www.sciencedirect.com
ScienceDirect
Journal of Solid State Chemistry 181 (2008) 905–912
JOURNAL OF SOLID STATE CHEMISTRY
www.elsevier.com/locate/jssc

Surface properties and performance for VOCs combustion of $LaFe_{1-y}Ni_yO_3$ perovskite oxides

G. Pecchi[a,*], P. Reyes[a], R. Zamora[a], L.E. Cadús[b], J.L.G. Fierro[c]

[a]*Departamento de Físico-Química, Facultad de Ciencias Químicas, Universidad de Concepción, Casilla 160-C, Concepción, Chile*
[b]*INTEQUI, UNSL-CONICET, Universidad Nacional de San Luis, Casilla 290, 5700 San Luis, Argentina*
[c]*Instituto de Catálisis y Petroleoquímica, CSIC, Cantoblanco, 28049 Madrid, Spain*

Received 25 October 2007; received in revised form 2 January 2008; accepted 6 January 2008
Available online 19 January 2008

Abstract

$LaFeO_3$, $LaNiO_3$ and substituted $LaFe_{1-y}Ni_yO_3$ ($y = 0.1$, 0.2 and 0.3) perovskites were synthesized by the citrate method and used in the catalytic combustion of ethanol and acetyl acetate. Chemical composition was determined by atomic absorption spectrometry (AAS) and specific areas from nitrogen adsorption isotherms. Structural details and surface properties were evaluated by temperature-programmed reduction (TPR), infrared spectroscopy (FTIR), X-ray diffraction analysis (XRD), temperature-programmed desorption of oxygen (O_2-TPD) and photoelectron spectroscopy (XPS). Characterization data revealed that total insertion of nickel in the $LaFeO_3$ takes place for substitution $y = 0.1$. However, NiO segregation occurs to some extent, specifically at higher substitutions ($y > 0.1$). The catalytic performance of these perovskites was evaluated in the combustion of acetyl acetate and ethanol. Among these molecules, ethanol exhibited the lowest ignition temperature, and the catalytic activity expressed as intrinsic activity ($mol\,m^{-2}\,h^{-1}$) was found to increase substantially with the nickel substitution. These results can be explained in terms of the cooperative effect of a $LaFe_{1-y}Ni_yO_3$ and NiO phases, whose relative concentration determines the oxygen activation capability and hence their reactivity.

Keywords: Iron; Nickel; Perovskites; Combustion; Ethanol; Acetyl acetate

1. Introduction

Since 1970s when perovskites, represented by the general formula ABO_3, were proposed as a promising automobile exhaust catalysts [1], they have been investigated as an alternative catalysts for deep oxidation of hydrocarbons. Investigation of these structures is important both for basic knowledge and for applications in domains in which materials involving electron transfer are of great interest. The consequences of a partial substitution of the cation B by B′ of similar oxidation state and ionic ratio may have interest to improve the stability or to enhance the redox efficiency of the perovskite. Possible applications of these systems in electrochemistry [1], superconductivity [2,3] and the intrinsic catalytic properties in different reactions such as: decomposition of H_2O_2 [4], steam reforming of methane [5] and catalytic total oxidation [6–8] have been reported. A report on the kinetic of combustion of methane over $LaCr_{1-x}Ni_xO_3$ perovskites [9] showed good stability up to substitution $x = 0.5$. For these systems, it was claimed that the oxygen atom bonded to two nickel atoms [Ni–O–Ni] is the active site for the combustion reaction.

It has been reported that the catalytic activity of perovskite type $AB_yB'_{1-y}O_3$, is related with the metal–oxygen bond and with the free energy of reduction of the cation placed at B and B′ sites [10]. Tabata et al. [11] have studied the difference electronic states of the perovskite-type $LaMn_{1-x}Cu_xO_{3+\lambda}$ oxides and concluded that the increase of the ionic character of the oxygen adsorbed is related to the non-stoichiometric oxygen. For these systems, the enhancement in the catalytic activity during CO oxidation has been explained in terms of a change in the electronic structure of the adsorbed oxygen (O^-) due to the nature of the cation B [11].

*Corresponding author.
E-mail address: gpecchi@udec.cl (G. Pecchi).

0022-4596/$ - see front matter © 2008 Elsevier Inc. All rights reserved.
doi:10.1016/j.jssc.2008.01.020

$LaFeO_3$ belongs to orthorhombic and $LaNiO_3$ to rhombohedral system, therefore a change from orthorhombic to rhombohedral takes place in the partially substituted $LaFe_{1-y}Ni_yO_3$ perovskites [12,13]. Although Asai et al. [14] reported that $LaFe_{1-y}Ni_yO_3$ solid solutions are only obtained for higher substitutions ($y>0.7$), a continuous range of solid solutions were found by other authors [15,16]. This work was undertaken with the aim to elucidate the structure and surface composition of substituted $LaFe_{1-y}Ni_yO_3$ perovskite oxides, in the low substitution range ($y=0.1$, 0.2 and 0.3), and their influence in VOCs removal.

2. Experimental

2.1. Preparation of the catalysts

Substituted $LaFe_{1-y}Ni_yO_3$ ($y=0.1$, 0.2 and 0.3) perovskites and $LaFeO_3$ and $LaNiO_3$ reference oxides were prepared by the citrate method [16]. Stoichiometric amounts of an aqueous solution of the nitrates of the corresponding metals were added to an aqueous solution of citric acid with a 10% of excess over the number of ionic equivalents of cations. The resulting solution was stirred for 15 min at room temperature and slowly evaporated at 343 K under vacuum in a rotary evaporator until gel formation was reached. Then this gel was dried in an oven, increasing slowly the temperature up to 523 K and maintaining it overnight to yield an amorphous citrate precursor. The resulting powder was crushed and sieved to obtain the required particle size (<200 μm) and calcined at 973 K in air for 6 h. The samples were labelled as $LaFe_{1-y}Ni_xO_3$, where $y = 0.0$, 0.1, 0.2, 0.3 and 1.0.

2.2. Characterization

Chemical analysis of samples was determined by atomic absorption spectrometry (AAS) using a Perkin Elmer instrument model 3100. Specific areas were calculated using the BET method from the nitrogen adsorption isotherms, recorded at the temperature of liquid nitrogen on a Micromeritics apparatus Model ASAP 2010, taking a value of 0.162 nm^2 for the cross-sectional area of the N_2 molecule adsorbed at 77 K. Prior to the adsorption measurements, samples were degassed at 423 K. X-ray powder diffraction (XRD) patterns were obtained with nickel-filtered Cu$K\alpha_1$ radiation ($\lambda = 1.5418$ Å) using a Rigaku diffractometer controlled by a computer. XRD diffraction profiles were collected in the 2θ range 5–80°, in steps of 2°/min. TPR and oxygen temperature-programmed desorption (TPD) experiments were performed in a TPR/TPD 2900 Micromeritics system provided with a thermal conductivity detector. Samples of about 20 mg were placed in a U-shape quartz tube first purged in a synthetic air stream of 50 mL/min at 773 K for 1 h and then cooled to ambient temperature. Reduction profiles were then recorded by passing a 5% H_2/Ar flow at a rate of 40 mL/min while heating at a rate of 10 K/min from ambient temperature to 1173 K. For the TPD experiments the samples were pretreated in an O_2 flow for 1 h at 973 K and then cooling down to room temperature in the same atmosphere. After switching the atmosphere by a helium flow, the sample was heated at constant rate of 10 K/min and the oxygen desorbed was monitored using a thermal conductivity detector. FTIR spectra were recorded in a Nicolet Magna-IR 550 instrument, equipped with a quartz sample holder with KBr windows. The samples were dehydrated at 483 K and finely ground in an agate mortar with KBr to obtain a sample/KBr ratio 1/150. Surface analysis was carried out on a VG Escalab 200R electron spectrometer provided with Mg$K\alpha$ X-ray source and a hemispherical electron analyser. Prior to analysis, all the samples were degassed at 573 K for 1 h within the pre-treatment chamber of the spectrometer. The binding energies were referenced to the C1 s peak at 284.9 eV due to adventitious carbon. Data processing was performed with the photoelectron spectroscopy (XPS) peak programme, the spectra were decomposed with the least squares fitting routine provided with the software with Gauss/Lorentz (90/10) curves and after subtracting a Shirley background. Atomic fractions were calculated using peak areas normalized on the basis of sensitivity factors.

2.3. Catalytic activity

The catalytic activity evaluation in the total combustion of acetyl acetate and ethanol was performed in a conventional flow reactor at atmospheric pressure. In each experiment, 100 mg of catalysts diluted with 100 mg of silica as an inert was used. The activity was measured at different temperatures. The reactant mixture was fed into the reactor at a rate of 100 mL/min. The temperature was linearly increased up to the required temperature, and then maintained constant for 30 min. Several isothermal steps were performed up to reach complete conversion. Both reactions were carried out under excess of oxygen, molar mixtures $C_4H_8O_2$:O_2:He = 1:10:89 and C_2H_5OH:O_2:He = 1:21:79. Effluents of the reactor were analysed using an on-line gas chromatograph Hewlett Packard model HP 4890D with thermal conductivity detector. A set of valves allowed bypass the reactor and feed directly the stream to the gas chromatography sampling loop, which provided a direct measurement of the VOC concentrations fed. Helium as carrier gas and a Supelco 25462 and Betadex 225 columns (30 m–0.5 mm) were used for permanent gas and VOC analysis, respectively. A Quadrupole mass spectrometer Shimadzu, GCMS-QP5050 model was used to detect small traces of products.

3. Results and discussion

3.1. Chemical composition and texture

The elemental composition of the perovskites was determined by AAS and results are compiled in Table 1.

It can be seen that nickel and lanthanum contents approach nominal ones although iron content is somewhat lower than the nominal composition. The rather low iron content is likely due to the high solubility of iron citrate, which keeps a fraction of iron in solution just before getting the mixed citrates gel during the drying step. As a consequence, part of the iron citrate could be lost during further handling steps. The specific BET areas of these samples are also summarized in Table 1. The largest BET area (20.9 m^2/g) is shown by the $LaFeO_3$ perovskite. Partial substitution of iron by nickel results in a progressive decrease in the value of BET area and reaches the lowest value (5.4 m^2/g) for substitution $y = 0.3$. The BET area again increases a little for the other $LaNiO_3$ reference (8.3 m^2/g) but in no case it reaches the value attained by the $LaFeO_3$.

3.2. Structural analysis

An XRD analysis of the calcined $LaFe_{1-y}Ni_yO_3$ oxides was performed with the objective to reveal crystalline phases developed during the calcination step. The XRD patterns of $LaFe_{1-y}Ni_yO_3$ oxides calcined at 973 K are displayed in Fig. 1. For comparison purpose, the bar patterns of orthorhombic $LaFeO_3$ (JC-PDF, 371493) and rhombohedral $LaNiO_3$ (JC-PDF, 330711) phases are also included. It can be seen that the $LaFeO_3$ and $LaNiO_3$ samples belong to orthorhombic and rhombohedral phases, respectively, with absence of any other crystalline phases [17,18]. A careful inspection of these diffraction profiles reveals some features: (i) a slight shift towards larger 2θ angles, due to lattice contraction, is observed upon substitution of Fe^{3+} ions in the lattice by Ni^{3+} ions and (ii) the full-width at half-maximum of diffraction lines increases upon substitution of Fe^{3+} by Ni^{3+}. These findings are in accordance with the general trend that the extent of nickel substitution is related to these effects and corresponds to some structure modification [19,20]. The peak shift towards higher 2θ angles as the nickel amount increases suggesting a decrease in the interplanar distance, i.e. the unit cell volume decreases due to the smaller by the presence of Ni^{3+}.

Provendier et al. [18] attributed the linear dependence of the lattice parameters with the substitution degree. The shift of the diffraction peaks corresponding to 2θ values of

Table 1
Bulk composition wt% (nominal values in brakets) and specific BET area for $LaFe_{1-y}Ni_yO_3$ perovskites

	y	La[a]	Fe[a]	Ni[a]	S_{BET}
$LaFeO_3$	0.0	64.2 (57.2)	18.0 (23.0)	–	20.9
La $Fe_{0.9}Ni_{0.1}O_3$	0.1	64.0 (57.2)	16.9 (20.7)	2.3 (2.3)	14.0
La $Fe_{0.8}Ni_{0.2}O_3$	0.2	64.5 (57.1)	15.6 (18.4)	4.8 (4.6)	8.3
La $Fe_{0.7}Ni_{0.3}O_3$	0.3	64.5 (57.0)	14.5 (16.0)	6.2 (6.9)	5.4
$LaNiO_3$	1.0	64.5 (56.6)	–	23.3 (22.7)	8.3

[a]Estimated error is below 1%.

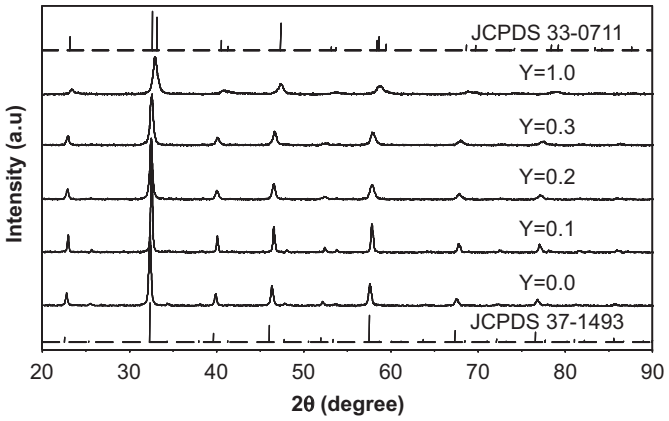

Fig. 1. X-ray diffraction patterns of $LaFe_{1-y}Ni_xO_3$ perovskites.

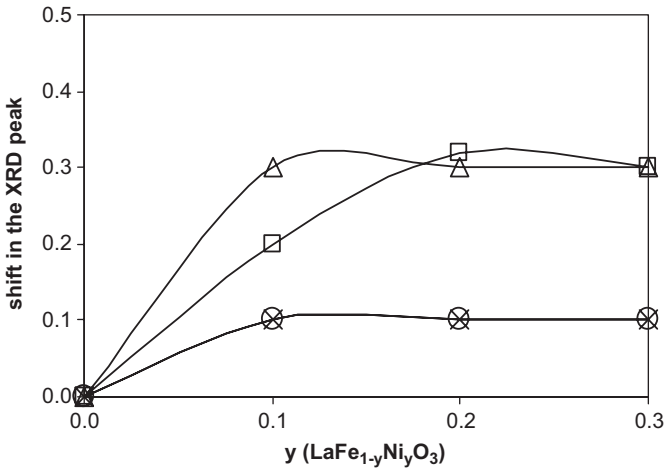

Fig. 2. Shift of the position of different diffraction peaks as a function of the substitution degree: (×) 32.3°, (○) 39.8°, (□) 46.2°, (△) 57.4°.

32.3°, 39.8°, 46.2° and 57.4° has been measured as a function of the degree of nickel substitution for all the prepared perovskites and the values are displayed in Fig. 2. It can be seen that, whatever be the peak chosen to analyse the effect, the trend is similar. The shift of the peak reaches a maximum for a substitution degree of $y = 0.1$ and then it remains constant for larger substitutions. This finding suggests that a complete insertion of nickel takes place for substitution $y = 0.1$, whereas a NiO_x phase becomes segregated for substitutions higher than 0.1. As a consequence, a certain proportion of separate, simple oxides should appear in parallel for substitutions $y > 0.1$. The absence of diffraction lines belonging to single iron or nickel oxides can be taken as indicative that these oxide phases are highly dispersed or in an amorphous form. It should be pointed out that the degree of substitution depends strongly on the preparation method. Thus, Provendier et al. [18] demonstrated that the sol–gel methodology allows to synthesize a continuous range of solid solutions between lanthanum ferrite and nickelate. Therefore, the preparation procedure affects significantly the uniformity of components in the final solid [22].

The infrared spectra of the samples are displayed in Fig. 3. The spectra of substituted $LaFe_{1-y}Ni_yO_3$ perovskites are similar to that of the orthorhombic $LaFeO_3$ structure but differ from the spectrum of rhombohedral $LaNiO_3$ structure, in which a large band attributed to bulk carbonates is detected. The t values was 0.84 for the substituted perovskites and 0.82 for $LaNiO_3$ [21]. In the orthorhombic structure, bands in the wavenumber regions 650–500 and 450–250 cm^{-1} arising from the asymmetric stretching vibrations of Fe–O–Fe bonds and deformation of FeO_6 octahedra, respectively, are observed [23]. It can be seen that on increasing nickel content to $y = 0.1$ the band at 560 cm^{-1} shifts to higher wavenumbers and increases in intensity compared to the one of pure $LaFeO_3$. This is indicative of electronic transitions [24]. Both band position and peak intensity have been quantified (results not shown). For substitutions $y = 0.2$ and 0.3 no significant changes either in the wavenumber or signal intensity are observed. The dependence of both parameters as a function of the substitution degree runs in parallel with the shift observed in the main diffraction lines of XRD patterns. These results are also conclusive that Ni^{3+} ions belong incorporated, within the perovskite structure.

3.3. Redox properties

Temperature-programmed reduction cycles (TPR_1–TPR_2) were performed with the aim to study the reducibility of the prepared perovskites, which is a key parameter to study the effect of nickel addition on the stabilization of the perovskite structure. The procedure included the following steps: (i) a first reduction step under H_2/Ar flow up to 973 K (TPR_1); (ii) cooling in Ar flow to room temperature; (iii) oxidation in an O_2/He flow mixture up to 973 K; and (iv) second reduction treatment (TPR_2) as in step (i) once the sample were cooled to ambient temperature. This procedure was selected to study the thermal stability of the prepared perovskites under hydrogen.

TPR profiles for the first and second reduction cycles for the studied perovskites are shown in Figs. 4 and 5, respectively. Non-substituted $LaFeO_3$ was found to be almost a non-reducible oxide under the TPR conditions employed in this work. Similar results have been reported by Provendier et al. [18] and Ciambelli et al. [19]. Substituted $LaFe_{1-y}Ni_yO_3$ perovskites did not show significant differences between TPR_1 and TPR_2 profiles, suggesting that their structure became restored after intermediate oxidation. In agreement with previous reports [18,19] distinct intensities are found in the two hydrogen-consumption peaks of $LaNiO_3$ perovskite sample. In the TPR_1 profile the intensity ratios of the first (610 K) to the second (769 K) reduction peak is 2:3, whereas in the TPR_2 the intensity of the first to the second peak is approximately 4:1. This result can be interpreted assuming that the first reduction peak corresponds to reduction of Ni^{3+} ions of $LaNiO_3$ to yield $La_2Ni_2O_5$ phase that obviously implies an oxygen loss from the structure [18]. The hydrogen consumption for this reduction fits with the corresponding reduction of Ni^{3+} to Ni^{2+}. The second peak with a maximum consumption of H_2 at 763 K leads to metallic nickel deposited on lanthanum oxide as it has been reported previously [4]. It can be noted that almost no reduction of $LaFeO_3$ takes place under the used conditions and no changes occur upon the hydrogen treatment.

A slightly different behaviour is found in the substituted perovskite with $y = 0.1$, in which only one small and broad

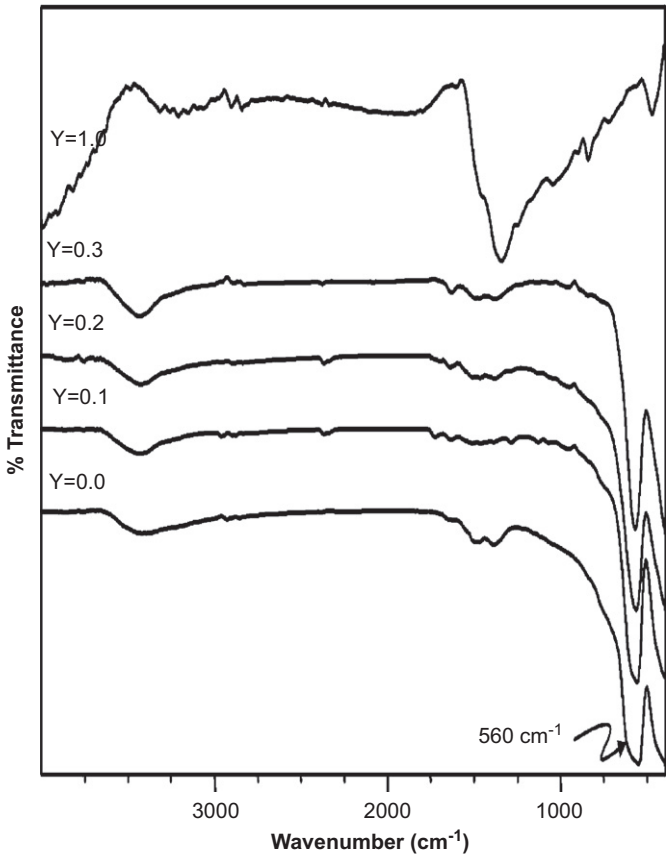

Fig. 3. FTIR spectra of $LaFe_{1-y}Ni_xO_3$ perovskites.

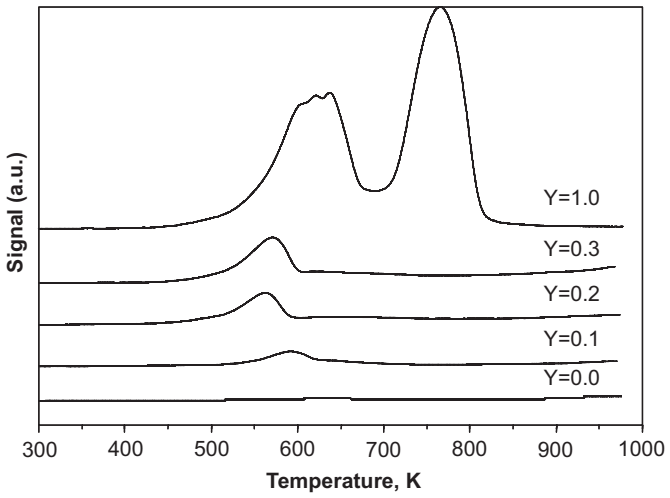

Fig. 4. Temperature-programmed reduction TPR_1 profiles of $LaFe_{1-y}Ni_xO_3$ perovskites.

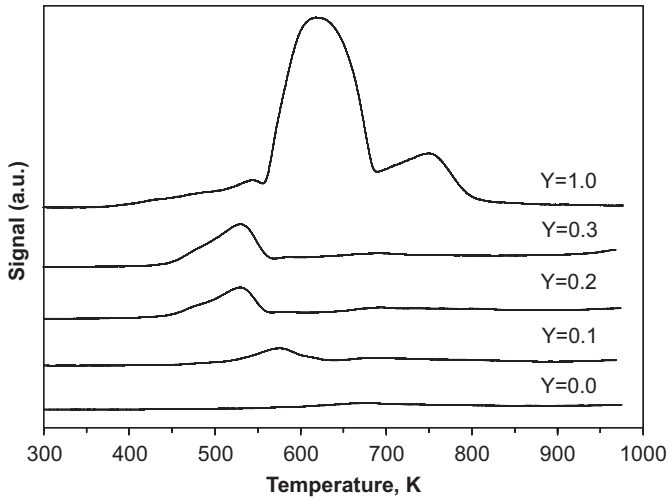

Fig. 5. Temperature-programmed reduction TPR_2 profiles of $LaFe_{1-y}Ni_xO_3$ perovskites.

peak with almost no change in intensity and hydrogen consumption is detected. This is indicative of the high stability of the $LaFeO_3$ and $LaFe_{0.9}Ni_{0.1}O_3$ samples. The other two substituted perovskites ($y = 0.2$ and 0.3) exhibit a similar behaviour, with only small changes in both TPR_1 and TPR_2 profiles. Thus, TPR_2 showed a slight shift towards lower reduction temperature, a shoulder in the reduction peak and a higher hydrogen consumption. Therefore, for these perovskites a partial reduction of Ni^{3+} to Ni^{2+} occurs during TPR_1, and thus the shoulder in the peak of the TPR_2 can be due to the reduction of segregated NiO crystallites. The appearance of a shoulder in the TPR_2 and its absence in the TPR_1 indicates that only a fraction of nickel incorporated into the perovskite structure is segregated from the crystal during TPR_1 and this fraction of nickel is re-oxidized into nickel oxide during oxidation step resulting in a mixture of perovskite and nickel oxide phases.

3.4. Surface properties

The evolution of oxygen during TPD experiments provide information dealing with the redox properties of these oxides [25]. Fig. 6 displays the O_2-TPD profiles. A common feature of these profiles is a low desorption peak centred at ca. 350 K, which comes likely from weakly bonded oxygen species. Similarly, a peak placed at low temperature has been previously reported for other substituted perovskites [6]. A second desorption peak at temperatures close to 500 K, commonly denoted α-oxygen, is shown by the non-substituted $LaNiO_3$ and the two substituted $y = 0.2$ and 0.3 samples. A significant enhancement in the intensity of this peak occurs as the degree of substitution increases. As this oxygen is related to the catalytic activity in oxidation processes, this result will be considered later in the discussion of catalytic results. In addition, another evolution of oxygen, takes place at 600 K

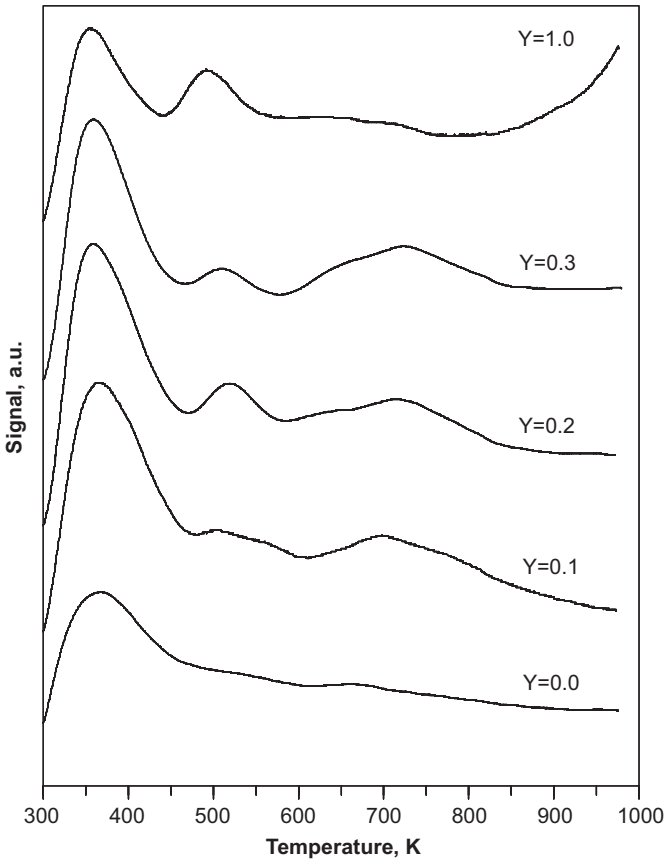

Fig. 6. Oxygen-temperature programmed desorption profiles of $LaFe_{1-y}Ni_xO_3$ perovskites.

on non-substituted $LaNiO_3$ sample and at 713 K on $LaFe_{1-y}Ni_yO_3$ perovskites with $y = 0.2$ and 0.3, denoted β-oxygen and associated with the lattice oxygen, is also observed. Notwithstanding the behaviour of O_2-TPD profiles of sample belonging to a substitution $y = 0.1$ is quite different as no desorption peak can be found. This agrees with the absence of segregated metal oxide phases in this sample. Finally, the profile of the non-substituted $LaFeO_3$ sample exhibits two broad and small oxygen desorption peaks at 504 and 697 K, similar to that shown by the substituted samples ($y = 0.2$ and 0.3). Thus, the O_2-TPD experiments revealed that samples desorb various oxygen species having differences in both intensity and temperature, specifically that related to the α-oxygen.

Further insight on the nature and relative abundance of surface species was revealed by photoelectron spectroscopy. Table 2 summarizes the binding energy values of C1*s*, La3$d_{5/2}$, Fe2$p_{3/2}$ and Ni2$p_{1/2}$ core-levels. Fig. 7a displays the O1*s* spectra of the samples. The O1*s* peak was fitted to three components, with a first one located at low binding energy (529.2 eV) assigned to surface O^{2-} species [26], a second one at 531.0 eV arising from lattice [La–O–M] bonds and the last one at 532.3 eV due to hydroxyl/carbonate groups [27]. No other O1*s* component at binding energies somewhat about 534 eV coming from adsorbed molecular water was found. This means that the

degassing procedure of samples (573 K for 1 h) is appropriate for molecular water removal from the surface. The C1*s* showed a high-binding energy component (289.0–289.2 eV) which is due to surface carbonates [28]. The binding energies of the most intense peaks of doublets for La3*d* (La3$d_{5/2}$) at 834.8 eV and Fe2*p* (Fe2$p_{3/2}$) at 710.3 eV and the least intense Ni2*p* (Ni2$p_{1/2}$) at 873.4 were almost constant in all the studied perovskites. Fig. 7b displays the Ni2$p_{1/2}$ of $LaFe_{1-y}Ni_xO_3$ perovskites. The satellite line placed at ca. 881.2 eV is indicative of the presence of Ni^{2+} ions on the surface. It is emphasized here that the higher BE contribution of the La3$d_{3/2}$ peak overlaps with the Ni2$p_{3/2}$ peak. This overlapping may mask not only the accurate measure of the BE of nickel but also its intensity. To overcome this complication, the Ni2$p_{1/2}$ was only measured and the corresponding binding energy values are given in Table 2. The percentage of O1*s* components as a function of the degree of substitution (*y*) are plotted in Fig. 8. It can be noted that the intensity of the peaks at 529.2 and 531.0 eV change almost linearly in a perfect opposite way. These changes can also be related to the incorporation of Ni in the structure as it was shown by DTP of oxygen. As will be shown below, the increase in intensity of the lattice oxygen component in the sample with larger Ni substitution can be related to higher catalytic activity in combustion reactions.

Table 2
Binding energies (eV) of core-levels for $LaFe_{1-y}Ni_yO_3$ perovskite oxides

	y	% Ni red	C 1*s*	La 3$d_{5/2}$	Fe 2$p_{3/2}$	Ni 2$p_{1/2}$
$LaFeO_3$	0.0	–	289.0	834.3	710.3	–
$La\ Fe_{0.9}Ni_{0.1}O_3$	0.1	7.1	289.0	834.4	710.2	873.5
$La\ Fe_{0.8}Ni_{0.2}O_3$	0.2	7.8	289.1	834.6	710.5	873.3
$La\ Fe_{0.7}Ni_{0.3}O_3$	0.3	13.1	289.0	834.5	710.4	873.3
$LaNiO_3$	1.0	8.9	289.2	834.6	–	873.4

Surface composition was calculated using atomic sensitivity factors according to Wagner et al. [29] for the Mg*K*α source. The surface atomic ratios Fe/La, Ni/La and CO_3^{2-}/La are displayed in Fig. 9. It can be observed that the Fe/La and Ni/La surface ratios are higher than the nominal compositions, and the differences are even larger upon increasing nickel substitution. In other words, the surface of the substituted perovskites becomes Ni- and Fe-enriched. The Fe/La surface ratio for the non-substituted $LaFeO_3$ is 0.959, which is consistent with the slight La-enrichment often reported for La-containing perovskites. On the opposite side is the Ni/La surface ratio of $LaNiO_3$ sample, which is 1.125, and also of the substituted $LaFe_{1-y}NiO_3$ samples. This finding is also conclusive that Ni^{3+} ions are more difficult to be stabilized than Fe^{3+} ions in the perovskite lattice, which results in surface segregation of a separate NiO phase. The extent of carbonation, as measured by the CO_3^{2-}/La atomic ratio is given in Fig. 9 as

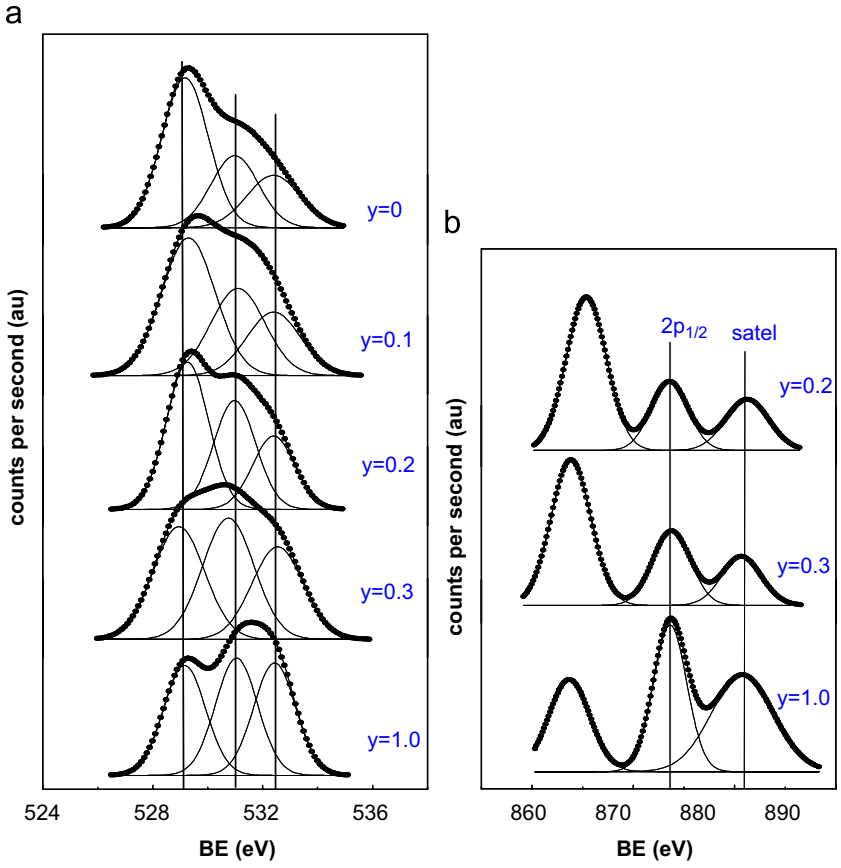

Fig. 7. O 1*s* (a) and Ni 2$p_{1/2}$ (b) core-level spectra of $LaFe_{1-y}Ni_xO_3$ perovskites.

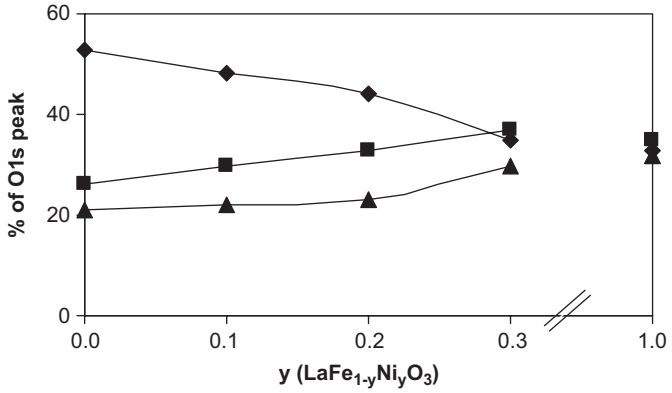

Fig. 8. Percent of O 1*s* binding energies for the $LaFe_{1-y}Ni_xO_3$ perovskites: (▲) 532.3 eV, (■) 531.0 eV, (◆) 529.2 eV.

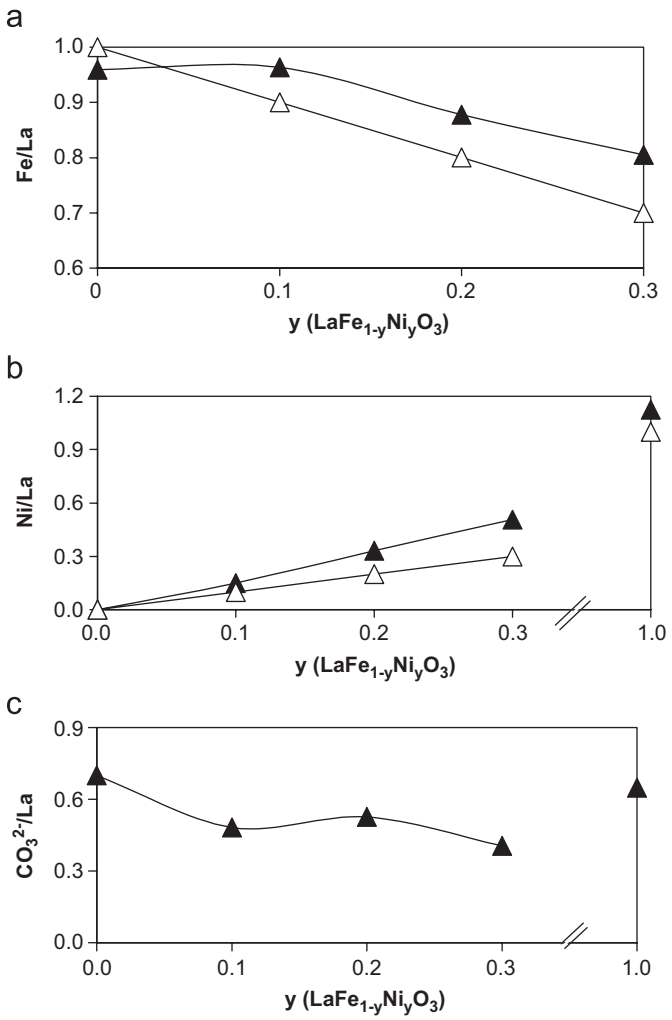

Fig. 9. XPS ratios for the $LaFe_{1-y}Ni_xO_3$ perovskites. (▲) atomic surface ratio, (△) nominal (a)Fe/La, (b) Ni/La, (c) CO_3^{2-}/La.

a function of the substitution degree. It can be seen that the extent of carbonation is higher for $LaFeO_3$, and is consistent with the slight La-enrichment observed in this sample. As a consequence of the basic character of lanthanum oxide, it tends to be carbonated by moisture. It can also be noted that the $y = 0.1$ substituted sample shows smaller differences between the bulk and surface ratios.

3.5. Catalytic activity

All the $LaFe_{1-y}Ni_yO_3$ samples were tested in acetyl acetate and ethanol combustion in a flow reactor under an excess of oxygen. Carbon dioxide and water were the only observed products for both combustion reactions at complete conversion, while trace amounts of acetaldehyde in the acetyl acetate and methanol in the ethanol combustion were also detected. The combustion profiles of ethanol and acetyl acetate conversion on the reaction temperature for a representative sample are displayed in Fig. 10. It is known that the main change in activity during oxidation of VOCs on perovskites when temperatures increases takes place at oxygen/substrate ratios lower than the stoichiometric ones. These changes in activity also occur with changes in the product distribution. However, oxygen/substrate ratio higher than the stoichiometric does not produces significant changes in activity, in line with the zero-order dependence on oxygen under those conditions. Differences in reactivity were found being the ethanol the one that reacts at lower temperature. The ignition temperature (T_{50}), defined as the temperature required to reach 50% conversion, and the intrinsic activity expressed as mmol converted per hour and square meter of catalyst evaluated at 523 K for acetyl acetate and 473 K for ethanol are compiled in Table 3. Similar activity trends were found under the experimental conditions. Thus, an increase in the reaction rate and parallel decrease in the ignition temperature of acetyl acetate and ethanol combustion was observed upon increasing the nickel substitution from 0 to 0.3. In the acetyl acetate and ethanol combustion, the total conversion was achieved at temperatures below 640 and 550 K, respectively. Table 3 also displays the values of the intrinsic activity, expressed as the rate of the oxidation at low

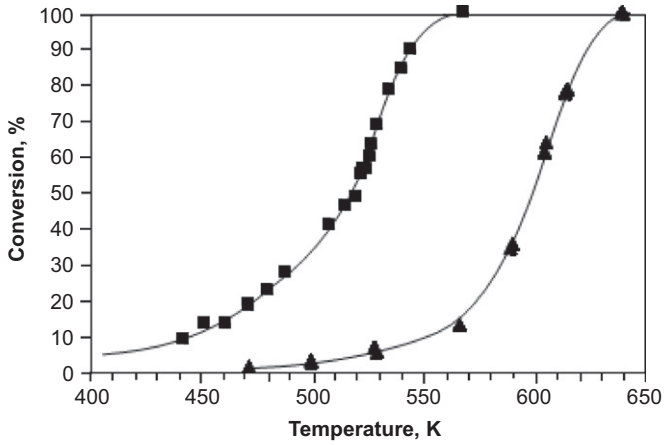

Fig. 10. Stationary-state conversion over $LaFe_{0.9}Ni_{0.1}O_3$ perovskites for: (■) ethanol, (▲) acetylacetate.

Table 3
Ignition temperature (T_{50}) and intrinsic activity at conversion level below 10% of ethanol and acetyl acetate on $LaFe_{1-y}Ni_yO_3$ perovskites

	y	T^{50}_{ign} (K)		Intrinsic activity ($mmol/m^2/h$)	
		Ethanol	Acetyl acetate	Ethanol 473 K	Acetyl acetate 523 K
$LaFeO_3$	0.0	520	613	0.012	0.010
$La\ Fe_{0.9}Ni_{0.1}O_3$	0.1	495	598	0.033	0.075
$La\ Fe_{0.8}Ni_{0.2}O_3$	0.2	491	566	0.12	0.12
$La\ Fe_{0.7}Ni_{0.3}O_3$	0.3	493	555	0.22	0.23
$LaNiO_3$	1.0	523	573	0.13	0.19

conversion level ($<10\%$). The results show a continuous increase in the reaction rate as Ni substitution increases and then it drops for the $LaNiO_3$. These results can be explained in terms of the cooperative effect of a $LaFe_{1-y}Ni_yO_3$ and NiO phases, whose relative concentration determines the oxygen activation capability and hence their reactivity for the oxidation of the organic compound. The approach undertaken in the present work of modulating the oxygen adsorption and release properties by inserting Ni^{3+} ions into the $LaFe_{1-y}Ni_yO_3$ structure while keeping a NiO separate phase is crucial to enhance the performance in the combustion of ethanol and acetyl acetate. Thus, the active sites may be related to the generation of sites associated to the presence of α-oxygen, in agreement with previous work on lanthanum-substituted manganites [30] for similar oxidation reactions.

4. Conclusions

$LaFeO_3$, $LaNiO_3$ and $LaFe_{1-y}Ni_xO_3$ perovskite-type oxides having moderate specific areas have been prepared by the citrate route. Characterization of bulk and surface structures by XRD, TPR, O_2-TPD, FTIR and XPS revealed that for substitution $y = 0.1$ the perovskite structure is maintained with no segregation of single oxides. At substitution degree (y) higher than 0.1, NiO phase segregation takes place. These perovskites have shown differences in catalytic behaviour depending on the nature of the substrate to be combusted, being ethanol the one that exhibits a higher reaction rate. A significant enhancement in catalytic activity, expressed as $mol\,m^{-2}h^{-1}$, with the nickel substitution was found. However, if the substitution of iron by nickel is complete the reaction rate drops. Thus, the modulation of oxygen adsorption and release properties by inserting Ni^{3+} ions into the $LaFe_{1-y}Ni_yO_3$ structure while keeping a NiO separate phase is crucial to enhance the performance in ethanol and acetyl acetate combustion reactions.

Acknowledgments

The authors thank CONICYT (FONDECYT Grant 1060702) and CONICET and the Universidad Nacional de San Luis from Argentina for financial support.

References

[1] R. Chiba, F. Yoshimura, Y. Sakurai, Solid State Ion. 124 (1999) 281.
[2] W.C. Koehler, E.O. Wollan, J. Phys. Chem. Solids 2 (1957) 100.
[3] S. Kawasakia, M. Takanoa, Y. Takedab, Solid State Ion. 108 (1998) 221.
[4] H. Falcón, R.E. Carbonio, J.L.G. Fierro, J. Catal. 203 (2001) 264.
[5] H. Provendier, C. Petit, A. Kienemann, C. R. Ácad. Sci. Ser. C 4A (2001) 57.
[6] N.A. Merino, B.P. Barbero, P. Grange, L.E. Cadús, J. Catal. 231 (2005) 232.
[7] Z. Yu, L. Gao, S. Yuan, Y. Wu, J. Chem. Soc. Faraday Trans. I 88 (1992) 3245.
[8] M.A. Peña, J.L.G. Fierro, Chem. Rev. 101 (2001) 1981, and references therein.
[9] K. Polawski, J. Lichtenberger, F. Keil, K. Schnitzlein, M. Amiridis, Catal. Today 62 (2000) 329.
[10] R. Sumathi, K. Johnson, B. Viswanathan, T.K. Varadarajan, Appl. Catal. A: Gen. 172 (1998) 15.
[11] K. Tabata, Y. Hirano, E. Suzuki, Appl. Catal. A: Gen. 170 (1998) 245.
[12] G.R. Herane, M.P. Paternak, R.D. Taylor, P. Lacorre, Phys. Rev. B 51 (1995) 11495.
[13] J.L. García Muñoz, J. Rodríguez Carvajal, P. Lacorte, J.B. Torrance, Phys. Rev. B 46 (1992) 4414.
[14] K. Asai, H. Sekisawa, J. Phys. Soc. Jpn. 49 (1980) 90.
[15] S. Aasland, H. Fjellvag, B.C. Hauback, J. Solid State Chem. 135 (1998) 103.
[16] P. Courty, H. Ajot, C. Marcilly, B. Delmon, Power Technol. 7 (1973) 21.
[17] E. Bontempi, C. Garzella, S. Valetti, L.E. Depero, J. Eur. Ceram. Soc. 23 (2003) 2135.
[18] H. Provendier, C. Petit, C. Estournes, S. Libs, A. Kienemann, Appl. Catal. A: Gen. 180 (1999) 163.
[19] P. Ciambelli, S. Cimino, L. Lisi, M. Faticanti, G. Minelli, I. Pettiti, P. Porta, Appl. Catal. B: Environ. 33 (2001) 193.
[20] R.D. Shannon, Acta Cryst. A 32 (1976) 751.
[21] V.M. Goldschmidt, Skr. Nor. Viedenk.-Akad., Kl. I: Mat.-Naturvidensk. Kl. 1926, No. 8.
[22] G. Pecchi, P. Reyes. R.Zamora. C. Campos, L.E.Cadús, B.P. Barbero, Catal. Today, in press, doi:10.1016/j.cattod.2007.11.011.
[23] A. Davydov, Infrared Spectroscopy of Adsorbed Species on the Surface of Transition Metal Oxides, Wiley, England, 1990 (Chapter 1).
[24] C. Roy, R.C. Budhani, J. Appl. Phys., 85(5), 3124 (1999) 22.
[25] M. Imamura, N. Matsubayashi, H. Shimada, J. Phys. Chem. B 104 (2000) 7348.
[26] L.G. Tejuca, J.L.G. Fierro, J.M.D. Tascón, Adv. Catal. 36 (1989) 237.
[27] Y.N. Lee, R.M. Lago, J.L.G. Fierro, V. Cortés, F. Sapiña, E. Martínez, Appl. Catal. A 207 (2001) 17.
[28] H. Taguchi, A. Sugita, M. Nagao, J. Sol. State Chem. 119 (1995) 164.
[29] C.D. Wagner, L.E. Davis, M.V. Zeller, J.A. Taylor, R.H. Raymond, L.H. Gale, Surf. Interface Anal. 3 (1981) 211.
[30] B.P. Barbero, J. Andrade Gamboa, L.E. Cadús, Appl. Catal. B: Environ. 65 (2006) 21.